Pramana – J. Phys. (2018) 90:62
https://doi.org/10.1007/s12043-018-1553-x

Parametrisation of the experimental fusion–fission cross-sections

H C MANJUNATHA* and N SOWMYA

Department of Physics, Government College for Women, Kolar 563 101, India
*Corresponding author. E-mail: manjunathhc@rediffmail.com

MS received 13 August 2017; revised 25 November 2017; accepted 27 November 2017;
published online 6 April 2018

Abstract. We have presented non-linear analytical formula for fusion–fission cross-sections. This is achieved by analysing many fusion–fission experiments of the compound nuclei of atomic number range $23 \leq Z \leq 146$ available in literature. Our parametrised formula can reproduce the fusion–fission cross-sections which agree well with the experiments. Our parametrisations depend on the charges and masses of the compound nuclei and fission fragments only. These results can be used as a guideline for estimating the fusion–fission cross-sections in those cases where measurements do not exist and also for studying new nuclei which are not yet explored.

Keywords. Superheavy nuclei; fusion–fission cross-sections.

PACS Nos 25.70.Jj; 24.10.–i

1. Introduction

A study of fusion–fission cross-sections for SHN is important for their synthesis. The synthesis of superheavy element involves three steps: two colliding nuclei fuse together by penetrating through the Coulomb barrier, compound nucleus will be formed and finally the excited compound nucleus by particle evaporation against fission will be survived. Nagame *et al* [1] measured the fusion–fission of heavy-ion reactions in ^{20}Ne and ^{50}Cr, ^{54}Cr. Scobel *et al* [2] measured cross-sections for fusion–fission of ^{35}Cl with ^{27}Al, ^{48}Ti, ^{54}Fe, ^{56}Fe, ^{58}Ni, ^{60}Ni, ^{62}Ni, ^{64}Ni, ^{90}Zr, and ^{116}Sn, ^{124}Sn. Sikora *et al* [2] analysed excitation functions obtained from semi-empirical fusion barriers. Guillaume *et al* [2] studied fission process for ^{32}S + ^{76}Ge reaction between 108 and 225 MeV. Coffin *et al* [2] studied strong damped reactions between nuclei and measured the fission fragments for ^{32}S + ^{59}Co reaction. Sikora *et al* [2] measured fission cross-sections for ^{168}Yb, ^{192,198,200}Pb, ^{210}Po, ^{213}Fr, and ^{251}Es nuclei by induced fusion reactions of ^{16}O, ^{18}O, ^{19}F, and ^{28,30}Si. Ademard *et al* [3] investigated decay modes of the excited nuclei in ^{78}Kr+^{40}Ca,^{82}Kr+^{40}Ca reactions at 5.5 MeV/nucleon. Charity *et al* [4] studied fusion–fission functions for the reactions by using ^{16}O and ^{19}F as projectiles to produce ^{158}Dy, ^{168}Yb, ^{178}W, ^{188}Pt, and ^{210}Po compound nuclei. Plasil *et al* [5] studied fission barrier of ^{153}Tb.

Torbjorn [6] measured fusion–fission cross-sections in the bombardment of Cs, Pr, Tb, Ho, Er, Tm, ^{174}Yb, Lu, ^{182}W, Au, and Bi with ^{16}O, Tm with ^{12}C, and Tb with ^{22}Ne. van der Plicht *et al* [2] measured fusion–fission cross-section excitation functions using ^{9}Be, ^{12}C, ^{16}O, ^{18}O, ^{24,26}Mg, ^{32}S, and ^{64}Ni beams. Gavron *et al* [2] studied fusion–fission cross-sections for compound nuclei such as ^{174}Yb, ^{198}Pt, ^{238}U, ^{142}Nd, ^{170}Er, ^{192}Os, ^{238}U, ^{126}Te, and ^{144}Nd. Zebelman *et al* [2] studied complete fission–fusion cross-sections for four channels leading to ^{170}Yb compound nuclei. Nishio *et al* [2] synthesised the isotopes of the element hassium using the reaction ^{34}S + ^{238}U → ^{272}Hs. Zebelman *et al* [7] reported fusion cross-sections in ^{11}B + ^{159}Tb, ^{12}C + ^{158} Gd, and ^{16}O + ^{154} Sm reactions resulting in ^{170}Yb. Tamain *et al* [8] reported fission–fusion cross-sections of argon-induced fission reaction. Logan *et al* [2] studied charged-particle emission for the reactions ^{40}Ar+^{116}Sn, ^{154}Sm, ^{164}Dy, and ^{197}Au. Delagrange *et al* [9] measured fusion–fission cross-sections in the reactions of ^{40}Ar with ^{116} Sn, ^{154}Sm, ^{164}Dy, and ^{197}Au. Britt *et al* [2] measured fusion–fission reactions such as ^{40}Ar+^{109}Ag, ^{40}Ar+^{121}Sb, and ^{84}Kr+^{65}Cu. Esterlund *et al* [10] determined fusion–fission cross-sections for the production of nuclides ^{132}Xe with Fe targets. Becchetti *et al* [2] measured the fission of nuclei with $159 \leq A \leq 232$ induced by the bombardment of ^{3}He ions. Huizenga *et al* [2,11] studied helium ion-induced fission cross-sections of bismuth, lead, thallium, and gold. Fomichve

et al [12] measured the fusion–fission cross-sections for the ^{4,6}He + ^{209}Bi reactions. Penionzhkevich *et al* [13] mentioned large cross-section observations below the Coulomb barrier for the production of ^{198}Au. Signorini *et al* [14] studied fusion cross-sections of ^{10,11}Be+^{209}Bi and compared with the stable system ^{9}Be + ^{209}Bi.

Dasgupta *et al* [2] measured the fusion–fission cross-sections for ^{6}Li + ^{209}Bi, ^{7}Li + ^{209}Bi, and ^{9}Be + ^{208}Pb reactions. Zuhua Liu *et al* [2] demonstrated experimentally that the reactions on the different side of Businaro–Gallone critical mass asymmetry have different characteristics in fusion–fission reactions. Appannababu *et al* [2] showed that the barrier energies are the same leading to compound nucleus ^{215}Fr for ^{11}B + ^{204}Pb and ^{18}O+^{197}Au reactions. Victor [15] measured total fission cross-sections for bombardment of ^{238}U with ^{4}He, ^{11}B, ^{12}C, ^{14}N, ^{16}O, and ^{20}Ne ions. Dasgupta *et al* [2] investigated complete fusion cross-sections for ^{9}Be incident on ^{208}Pb and ^{209}Bi. Gasques *et al* [2] examined the barrier cross-sections of fission and α-active heavy reaction products for the reactions of ^{10,11}B with ^{209}Bi. Ralarosy *et al* [2] gave a brief description of the experimental techniques to measure fusion–fission cross-sections. Mukherjee *et al* [2] showed that the fusion cross-sections at high energies differ significantly from the existing fusion data. Kushal Kalita [16] measured fission cross-sections for ^{12,13}C+^{208,207}Pb. Meyer *et al* [2] measured the fusion–fission cross-sections for ^{4}He + ^{233}U and ^{4}He + ^{209}Bi.

Shrivastava *et al* [17] studied the fusion–fission fragment anisotropies for ^{12}C + ^{198}P. Vigdor *et al* [18] investigated the decay of compound nuclei formed at high excitation and angular momentum in ^{6}Li bombardment of ^{181}Ta, ^{194,198}Pt, ^{197}Au, and ^{208}Pb. Laveen *et al* [19] analysed fusion–fission cross-sections for the reaction ^{18}O + ^{194}Pt. Mahata *et al* [20] examined fission fragment angular distributions in ^{19}F + ^{188,192}Os systems. Hinde *et al* [21] measured the fusion–fission of compound nuclei such as ^{168}Yb, ^{192,198,200}Pb, ^{210}Po, ^{213}Fr, and ^{251}Es. Uhl [2] has shown that ternary fission is induced in ^{209}Bi and ^{239}Pu with helium ions. Trotta *et al* [22] studied quasifission of some ^{48}Ca-induced reactions. Jack *et al* [2] measured fission cross-sections of ^{169}Tm + ^{11}B, ^{175}Lu + ^{11}B, and ^{12}C, ^{174}Y + ^{12}C, ^{182}W + ^{12}C, ^{165}Ho + ^{14}N, and ^{159}Tb + ^{19}F for energies up to 10.4 MeV per nucleon. Tripathi *et al* [2] investigated the contribution of non-compound nucleus fission in the reactions ^{16}O + ^{188}Os and ^{28}Si + ^{176}Yb. Tripathi *et al* [2] measured angular distribution of fission fragments for ^{19}F + ^{197}Au reaction. Videbaek *et al* [2] examined cross-sections for the quasielastic and fission channels in reactions of ^{16}O on ^{181}Ta and ^{208}Pb. Bivash *et al* [23] studied fusion–fission fragment angular distributions and cross-section for the system ^{16}O + ^{181}Ta. Mahata *et al* [24] measured fusion–fission reaction for ^{19}F + ^{194}Pt and ^{198}Pt.

Forster *et al* [25] measured the fusion–fission of some Pb nuclei. Ikezoe *et al* [2] measured pre- and post-scission of ^{4}He particle multiplicities for the ^{19}F+^{197}Au reaction. Piasecki *et al* [2] measured fusion–fission barrier distributions for ^{20}Ne + ^{208}Pb. Hinde *et al* [26] studied the formation of ^{200}Pb in both ^{19}F + ^{181}Ta and ^{30}Si + ^{170}Er reactions. Miller *et al* [27] produced compound nuclei ^{194}Hg from the reactions of ^{12}C and ^{19}F. Rajagopalan *et al* [2] produced twelve reactions of compound systems for ^{194}Hg. Morton *et al* [2] measured fusion–fission cross-sections for the reaction ^{34}S + ^{168}Er. Glagola *et al* [2] showed that the sub-barrier fusion–fission cross-sections strongly depend on the target deformation. Caraley *et al* [2] measured angular distributions of fusion–fission fragments. Knyazheva *et al* [2] measured mass–energy and angular distributions of fusion–fission fragments for ^{48}Ca + ^{144,154}Sm → ^{192,202}Pb and ^{40}Ca + ^{154}Sm → ^{194}P. Clerc *et al* [28] measured fusion–fission cross-sections for the reactions ^{40}Ar + ^{165}Ho and ^{50}Ti + ^{208}Pb. Cabrera *et al* [29] measured fusion–fission cross-sections for ^{20}Ne + ^{159}Tb and ^{20}Ne + ^{169}Tm reactions. Back *et al* [30] measured fusion–fission of ^{32}S and ^{144,154}Sm which exhibit a strong dependence on the deformation of target nucleus.

Lesko *et al* [31] measured fusion–fission cross-sections for the nuclei $^{170-188}$Pt formed by the reactions ^{58,64}Ni + $^{112-124}$Sn. Wolfs *et al* [32] measured fusion–fission yields for ^{58}Ni + ^{124}Sn at 230 and 290 MeV. Kohley *et al* [33] studied fusion–fission excitation functions for ^{132}Sn + ^{58}Ni and ^{130}Te + ^{58,64}Ni. Borderie *et al* [34] analysed possible mechanism in heavy-ion-induced reactions. Blann *et al* [2] reported fusion–fission cross-sections for ^{56}Fe + ^{120,122}Sn. Herbach *et al* [35] experimented ternary fission of heavy elements with energy in the reactions of ^{14}N with ^{197}Au and ^{232}Th. Bangert *et al* [36] studied reactions of ^{132}Xe with ^{56}Fe. Freiesleben *et al* [37] measured fusion–fission cross-sections for α-particle-induced fission of ^{233,238}U at 15–27 MeV. Trotta *et al* [38] measured fusion–fission cross-sections for ^{4}He + ^{238}U and ^{6}He + ^{238}U. Huizenga *et al* [39] measured fusion–fission cross-sections for ^{233}U and ^{238}U targets when bombarded with 18–43 MeV helium ions. Alain Fleury *et al* [2] determined fusion–fission cross-sections of ^{4}He with ^{237}Np, ^{237g}Am, ^{238g}Am, ^{238m}Am, ^{239g}Am, ^{239m}Am, and ^{240g}Am.

Raabe *et al* [41] observed strong increase of the fusion probability for heavy deformed nuclei. Bethune *et al* [2] measured fusion–fission cross-sections for the ^{235}U, ^{236} Pu, ^{235}U, ^{236}Np, and ^{235}U reactions between 24.5 and 28.0 MeV. A sub-nanosecond fission isomer was detected in ^{238}Pu by means of fission-inflight technique [42]. Gunnink *et al* [43] measured fusion–fission yield of

approximately 25 nuclides from the helium-ion-induced fission of ^{235}U. Colby *et al* [44] measured fusion–fission cross-sections of ^{233}U and ^{238}U. Parihari *et al* [2] studied fusion–fission angular distributions for ^{6,7}Li + ^{235,238}U reaction. Fekou-Youmbi *et al* [45] measured relative fusion–fission cross-sections for ^{9}Be+^{238}U and ^{11}Be + ^{238}U. Fekou *et al* [46] showed that the nuclear structure of halo nuclei may have strong influence on fusion cross-sections. Ramamurthy *et al* [47] measured fission angular distributions in reactions of ^{10}B, ^{12}C, ^{16}O+^{232}Th, ^{237}Np, and ^{19}F+^{237}Np. Nadkarni *et al* [2] measured fission cross-sections for the systems of ^{11}B, ^{16}O, ^{19}F+^{232}Th. Tripathi *et al* [48] carried out an experiment for fusion–fission reactions in ^{11}B + ^{243}Am in the energy range 60–72 MeV. Ajith Kumar *et al* [2] reported fusion–fission cross-sections for ^{13}C + ^{232}Th. Bivash *et al* [2] reported fusion–fission cross-sections for the systems of ^{11}B + ^{235}U and ^{14}N + ^{232}Th. Vulgaris *et al* [2] measured fusion–fission transfer for ^{16,18}O + ^{208}Pb and ^{15}N, ^{16}O + ^{209}Bi. Karnik *et al* [49] fitted fission excitation function by deducing Wong model. Dasgupta *et al* [50] proposed gradual decoherence to allow a consistent description of nuclear fusion. Kailas *et al* [2] observed that the largest ratio of the transfer fission to the total fission is around 10 to 15%.

Rehm *et al* [51] measured the fusion–fission cross-section for the system ^{17}F + ^{208}Pb. Zhang Huanqiao *et al* [52] investigated the fusion–fission cross-section for the system ^{19}F + ^{208}Pb. Huanqiao Zhang *et al* [53] measured the fusion–fission cross-section for the system ^{19}F + ^{232}Th. Morton *et al* [2] calculated fission fragment for anisotropies using the transition state model. Shen *et al* [2] measured fusion–fission reaction in U-induced reactions. Back *et al* [2] measured fusion–fission cross-sections for ^{16}O + ^{208}Pb, ^{232}Th, ^{238}U, ^{248}Cm; ^{19}F + ^{208}Pb; ^{24}Mg + ^{208}Pb,^{28}Si + ^{208}Pb; ^{32}S + ^{197}Au and ^{32}S + ^{208}Pb. Watanabe *et al* [54] measured fusion–fission cross-sections for three isotopes ^{27,29,31}Al bombarding a ^{197}Au target. Sann *et al* [55] measured fusion–fission cross-sections in bombardments with ^{208}Pb on targets of ^{26}Mg, ^{27}Al, ^{48}Ca, ^{50}Ti, ^{52}Cr, and ^{58}Fe. Reich *et al* [56] studied fusion–fission cross-section of ^{23}Na + ^{206}Pb. Samant *et al* [57] measured fission fragment angular distributions for ^{19}F+^{209}Bi. Bock *et al* [58] studied binary reaction products from the interaction of ^{208}Pb with targets of ^{26}Mg, ^{27}Al, ^{48}Ca, ^{50}Ti, ^{52}Cr, ^{58}Fe, and ^{64}Ni.

Yanez *et al* [2] measured the fusion–fission cross-section of ^{18}O, ^{26}Mg, ^{30}Si, ^{36}S with ^{197}Au. Williams *et al* [2] measured quasifission cross-section for ^{12}C + ^{232}Th, ^{30}Si + ^{208}Pb, ^{32}S + ^{202}Hg, ^{48}Ti + ^{186}W, and ^{64}Ni + ^{170}Er. Hinde *et al* [59] showed that collision of ^{16}O with ^{238}U results in fission–fusion process. Nishio *et al* [2] measured fusion–fission cross-section for ^{28}Si + ^{198}Pt. Hinde *et al* [2] reported experimental fusion–fission cross-sections for ^{32}S + ^{208}Pb, ^{34}S + ^{206}Pb, and ^{36}S + ^{204}Pb. Khuyagbaatar *et al* [2] measured the fusion–fission cross-sections for the reactions ^{34}S+^{204,206,208}Pb and ^{36}S+^{204,206,208}Pb. Hinde *et al* [2] studied ^{7}Li, ^{16}O, and ^{20}N-induced fusion–fission reactions in ^{142}Nd, ^{168}Er, ^{181}Ta, ^{197}Au, ^{209}Bi, and ^{232}Th.

Mitsuoka *et al* [2] observed that fusion of ^{60}Ni + ^{154}Sm and ^{32}S + ^{182}W reactions lead to the same compound nucleus ^{214}Th. Loveland *et al* [60] measured the fusion–fission excitation functions for the ^{32}S + ^{181}Ta and ^{38}S + ^{181}Ta reactions. Ngo *et al* [61] studied the fusion of Ar+Au system at two energies 201 and 248 MeV. Back *et al* [2] studied the fusion reactions for ^{32}S+^{182}W, ^{48}Ti+^{166}Er, and ^{60}Ni+^{154}Sm, all of which will lead to the compound system ^{214}Th. Experimental fusion–fission of ^{236}U is reported in [62]. Bierman *et al* [2,63] presented fusion excitation functions for the two systems ^{40}Ca + ^{192}Os, ^{194}Pt. Viola *et al* [64] studied fusion for ^{20}Ne + ^{235}U at 175 MeV and 252 MeV. Zyromski *et al* [2] measured the capture-fission excitation functions for the reactions ^{32}S + ^{181}Ta and ^{38}S + ^{181}Ta. Vinodkumar *et al* [2] analysed fusion data for ^{16}O + ^{16}O by coupled channels. Tsang *et al* [2] measured fission fragment mass and angular distributions for ^{32}S-induced reactions on ^{208}Pb. Pacheco *et al* [2] analysed capture-fission cross-sections for ^{40,48}Ca + ^{197}Au and ^{40,48}Ca + ^{208}Pb. Louis *et al* [65] studied the fusion–fission reactions of ^{16}O with ^{12}C, ^{181}Ta, ^{208}Pb, and ^{238}U. Prokhorova *et al* [66] studied mass– energy distributions and capture fission cross-sections for ^{48}Ca + ^{208}Pb. Ngo *et al* [67] investigated the fusion of Ar+Au system.

Zheng *et al* [68] studied the fusion–fission products for three reactions Ar+Au, Ar+Bi, and Ar+U. Keller *et al* [2] studied the fusion reaction ^{32}S + ^{182}W. Birkelund *et al* [2] studied the fusion–fission reaction of ^{165}Ho + ^{56}Fe. Morrissey *et al* [69] reported radioanalytical mass yield distribution for the fusion–fission reaction of ^{48}Ca + ^{208}Pb. Cross-sections for quasifission are measured for the systems Kr+Ho, Kr+W, Kr+Bi, Kr+U in the energy range 450–525 MeV [70]. Katsuhisa [71] studied the fusion–fission of ^{239}Pu. Itkis *et al* [72] obtained mass and energy distributions of fission-like fragments in the reaction ^{26}Mg, ^{36}S, and ^{58}Fe ions leading to the formation of $Z = 108$. Toke *et al* [73] studied the fission of ^{238}U with their fragments of ^{16}O, ^{27}Al, ^{48}Ca, ^{45}Sc, ^{48}Ti, ^{58}Fe, ^{64}Ni, and ^{89}Y. Toke *et al* [74] measured quasifission fragment yields for ^{238}U + ^{16}O. Nishio *et al* [75] studied the fusion–fission of ^{30}Si + ^{238}U, ^{30}Si + ^{238}U, ^{40}Ca + ^{238}U, and ^{48}Ca + ^{238}U. Freifelder *et al* [2] studied the total capture cross-section for the ^{32}S + ^{238}U system. Franz *et al* [76] measured integral cross-sections for fission in the ^{132}Xe+^{238}U system. Literature survey shows that many

experimental fusion–fission cross-sections are available for different projectile–target combinations at different energies. In the present work, we have made an attempt to parametrise the available experimental fusion–fission cross-sections.

2. Theory

Once the experimental fusion–fission cross-sections were extracted from different experiments available in the literature, a search was made for their parametrisation. Since it is evident that fusion–fission depend on the size of the splitting fragments, the best way is to parametrise them in terms of the radius dependence, i.e. in terms of $A^{1/3}$. It is also evident from the literature that fusion–fission cross-section inversely depends on energy $E_{\rm cm}$. Fusion–fission process also depends on the quantity Z^2/A. By considering these facts, we have constructed a new function (Y) for parametrisation of fusion–fission cross-section. This function depends on the atomic number and mass number of the compound nucleus and fission fragments.

$$Y = \left(\frac{r_c^2}{E_{\rm cm}}\right) \times \left(\frac{Z^2}{A}\right) \times \left(\frac{(A_1A_2)^{1/3}}{A_1^{1/3} + A_2^{1/3}}\right), \qquad (1)$$

where A, A_1 and A_2 are mass numbers of the compound nucleus and fission fragments respectively. Z and A are atomic number and mass number of the compound nuclei.

$$r_c = D_1 + D_2 + 1.44,$$

where

$$D_1 = R_1 - \left(\frac{1}{R_1}\right) \quad \text{and} \quad D_2 = R_2 - \left(\frac{1}{R_2}\right).$$

and

$$R_2 = 1.28A_2^{1/3} - 0.76 + 0.8A_2^{-1/3}.$$

Based on the function defined in eq. (1), a search was made for the parametrisation of available experimental fusion–fission cross-sections.

2.1 *Fusion–fission cross-section for atomic number range* $23 \le Z \le 56$ *in the energy region* 0–500 *MeV*

A detailed study of the variation of fusion–fission cross-section with the defined function (Y) reveals that fusion–fission cross-section may be expressed in terms of polynomial functions. Thus, fusion–fission cross-section for different fragment combinations of the compound nuclei of atomic number range $23 \le Z \le 56$ is parametrised for different energy ranges as follows:

$$\sigma_{\rm FF}\,({\rm mb}) = \begin{cases} 6.19954 + 0.00999Y - 6.25785 \times 10^{-6}Y^2 & \\ \quad +1.60743 \times 10^{-9}Y^3 - 1.02961 \times 10^{-13}Y^4 & \text{for } \ 0 \le E_{\rm cm} \le 150\,{\rm MeV} \\ -0.2590508722Y + 27.39176097\sqrt{Y} - 331.4284961 & \text{for } \ 150 \le E_{\rm cm} \le 500\,{\rm MeV} \end{cases}$$

In the above equation, Y is the function defined in eq. (1). This equation is applicable to the fusion–fission cross-section of the compound nuclei of atomic number range $23 \le Z \le 56$.

2.2 *Fusion–fission cross-section for atomic number range* $57 \le Z \le 71$ *(lanthanides) in the energy region* 80–800 *MeV*

We have studied the variation of fusion–fission cross-section with the defined function (Y). The variation of fusion–fission cross-section with the defined function (Y) is linear, rational, logarithmic, and quadratic for different energy regions. Fusion–fission cross-section for different fragment combinations of compound nuclei of atomic number range $57 \le Z \le 71$ parametrised for different energy ranges are as follows:

$$\sigma_{\rm FF}({\rm mb}) = \begin{cases} -3.933521 \times 10^{-7}Y + 5.2916038 & \text{for } 80 \le E_{\rm cm} \le 100\,{\rm MeV} \\ 264.771261 \times Y - 1760717.168/Y & \text{for } 100 \le E_{\rm cm} \le 120\,{\rm MeV} \\ -144553684.2/Y + 44.07264 & \text{for } 120 \le E_{\rm cm} \le 130\ {\rm MeV} \\ -14.6822\ln(Y) + 312.6613 & \text{for } 130 \le E_{\rm cm} \le 160\,{\rm MeV} \\ 33.4363\ln(Y) - 350.8888 & \text{for } 160 \le E_{\rm cm} \le 200\,{\rm MeV} \\ -6.6555 \times 10^{-5}Y + 0.37456\sqrt{Y} + 2.12769 & \text{for } 200 \le E_{\rm cm} \le 800\,{\rm MeV} \end{cases}$$

In the above equation, Y is the function defined in eq. (1). This equation is valid for atomic number range $57 \le Z \le 71$ and energy up to 800 MeV.

Here

$$R_1 = 1.28A_1^{1/3} - 0.76 + 0.8A_1^{-1/3}$$

2.3 *Fusion–fission cross-section for atomic number range* $72 \leq Z \leq 88$ *in the energy region* 0–1200 *MeV*

Fusion–fission cross-section for different fragment combinations of compound nuclei of atomic number range $72 \leq Z \leq 88$ parametrised for different energy ranges are as follows:

In this equation, Y is the function defined in eq. (1). α_i, β_i, and δ_i are fitting parameters which are given in table 1. This equation is valid for atomic number range $89 \leq Z \leq 103$ and energy up to 1200 MeV. The parametrised function for fusion–fission cross-section in terms of the defined function (Y) is the power function in the low-energy region

$$\sigma_{\mathrm{FF}}\,(\mathrm{mb}) = \begin{cases} 318.8781611 \times \mathrm{e}^{-81713014.55/Y} & \text{for } 0 \leq E_{\mathrm{cm}} \leq 30\mathrm{MeV} \\ -4.965015655 \times 10^{-7}Y + 23.07597411 & \text{for } 30 \leq E_{\mathrm{cm}} \leq 45\mathrm{MeV} \\ -0.01586394379\sqrt{Y} + 187.459168 & \text{for } 45 \leq E_{\mathrm{cm}} \leq 65\,\mathrm{MeV} \\ -4.236929826 \times 10^{-6}Y + 207.3377261 & \text{for } 65 \leq E_{\mathrm{cm}} \leq 80\,\mathrm{MeV} \\ 142.1143659Y/(Y + 2847620.913) & \text{for } 80 \leq E_{\mathrm{cm}} \leq 90\,\mathrm{MeV} \\ 335.8835705 \times \mathrm{e}^{-8509784.163/Y} & \text{for } 90 \leq E_{\mathrm{cm}} \leq 105\,\mathrm{MeV} \\ -6.280655738 \times 10^{-6}Y + 457.8571071 & \text{for } 105 \leq E_{\mathrm{cm}} \leq 120\,\mathrm{MeV} \\ -7.667965528 \times 10^{-6}Y + 600.6366236 & \text{for } 120 \leq E_{\mathrm{cm}} \leq 140\,\mathrm{MeV} \\ -8.787591672 \times 10^{-6}Y + 919.7165001 & \text{for } 140 \leq E_{\mathrm{cm}} \leq 190\,\mathrm{MeV} \\ -7.066127958 \times 10^{-6}Y + 1182.810567 & \text{for } 190 \leq E_{\mathrm{cm}} \leq 1200\,\mathrm{MeV} \end{cases}$$

The parametrised function for fusion–fission cross-section in terms of the defined function (Y) is Gaussian in the low-energy region up to 30 MeV. The parametrised function for fusion–fission cross-section is linear for the energy range 30–1200 MeV except some energy regions (80–105 MeV). The fusion–fission cross-section functions are rational and Gaussian for the 80–90 MeV and 90–105 MeV energy region. In the above equation, Y is the function defined in eq. (1). This equation is valid for atomic number range $72 \leq Z \leq 88$ and energy up to 1200 MeV.

2.4 *Fusion–fission cross-section for atomic number range* $89 \leq Z \leq 103$ *(actinides) in the energy region* 0–1200 *MeV*

Fusion–fission cross-section for different fragment combinations of compound nuclei of atomic number range $89 \leq Z \leq 103$ parametrised for different energy ranges are as follows:

up to 30 MeV. The parametrised function for the fusion–fission cross-section in terms of Y is Gaussian for the energy regions 60–100 MeV. This function is fourth- and third-order polynomial functions for the energy regions 30–60 MeV and 100–200 MeV respectively. The fusion–fission cross-section is also parametrised as logarithmic for the energy region 200–1200 MeV.

2.5 *Fusion–fission cross-section for atomic number range* $104 \leq Z \leq 146$ *(superheavy nuclei) in the energy region* 0–900 *MeV*

The variation of fusion–fission cross-section is studied with the newly defined function (Y). This variation may be expressed as the sum of the Gaussian functions. Thus, we parametrised fusion–fission cross-section for different fragment combinations of compound nuclei of atomic number range $104 \leq Z \leq 146$ for energy up to 900 MeV as follows:

$$\sigma_{\mathrm{FF}}\,(\mathrm{mb}) = \begin{cases} 0.1066838774Y^{5344699.254/Y} & \text{for } 0 \leq E_{\mathrm{cm}} \leq 30\,\mathrm{MeV} \\ \sum_{i=0}^{4} \alpha_i y^i & \text{for } 30 \leq E_{\mathrm{cm}} \leq 60\,\mathrm{MeV} \\ 5.574817131 \times \exp(146752601.7/Y) & \text{for } 60 \leq E_{\mathrm{cm}} \leq 80\ \mathrm{MeV} \\ 9.050833396 \times \exp(141843355/Y) & \text{for } 80 \leq E_{\mathrm{cm}} \leq 100\,\mathrm{MeV} \\ \sum_{i=0}^{3} \beta_i Y^i & \text{for } 100 \leq E_{\mathrm{cm}} \leq 150\,\mathrm{MeV} \\ \sum_{i=0}^{3} \delta_i Y^i & \text{for } 150 \leq E_{\mathrm{cm}} \leq 200\,\mathrm{MeV} \\ -605.9364065\ln(Y) + 11762.8265 & \text{for } 200 \leq E_{\mathrm{cm}} \leq 1200\,\mathrm{MeV} \end{cases}$$

Table 1. Fitting parameters for fusion–fission cross-section of atomic number range $89 \leq Z \leq 103$.

i	α_i	β_i	δ_i
0	1813.177874	2808.450946	2771.49021
1	$-1.073182947 \cdot 10^{-4}$	$-5.518093195 \cdot 10^{-5}$	$-4.507597225 \cdot 10^{-5}$
2	$2.729969695 \cdot 10^{-12}$	$3.234871922 \cdot 10^{-13}$	$2.470557882 \cdot 10^{-13}$
3	$-3.344942386 \cdot 10^{-20}$	$-4.776232112 \cdot 10^{-22}$	$-4.413784863 \cdot 10^{-22}$
4	$1.600742004 \cdot 10^{-28}$	–	–

$$\sigma_{\mathrm{FF}}\,(\mathrm{mb}) = \left\{2028.65005 \times \exp\left(\frac{-Y}{6.65891 \times 10^{7}}\right)\right.$$
$$+58.53013 \times \exp\left(\frac{-Y}{-8.66343 \times 10^{32}}\right)$$
$$\left.-12.54312 \times \exp\left(\frac{-Y}{1.4304 \times 10^{43}}\right)\right.$$

In the above equation, Y is the function defined in eq. (1).

3. Results and discussion

Using the available experimental data, we obtained non-linear analytical relations for fusion–fission cross-sections. Our analysis is based on the experimental cross-sections. Parametrisation of fusion–fission cross-section of the compound nuclei of $23 \geq Z \geq 56$ considered the 41 experimental fusion–fission reactions of different energy ranges available in the literature. The coefficient of determination $\langle R^2 \rangle$ of the experimental values by the present formula is 0.98. Parametrisation of fusion–fission cross-section of the compound nuclei of $57 \geq Z \geq 71$ considered 168 experimental fusion–fission reactions of different energy ranges available in the literature. The coefficient of determination $\langle R^2 \rangle$ of the experimental values by the present formula is 0.97.

Parametrisation of the fusion–fission cross-section of the compound nuclei of $72 \geq Z \geq 88$ considered 1468 experimental fusion–fission reactions of different energy ranges available in the literature. The coefficient of determination $\langle R^2 \rangle$ of the experimental values by the present formula is 0.96. Similarly, we have considered 1689 and 181 experimental fusion–fission reactions for parametrisation of fusion–fission cross-section of the compound nuclei of $89 \geq Z \geq 103$ and $104 \geq Z \geq 146$ respectively. The corresponding coefficients of determination $\langle R^2 \rangle$ of experimental values by the present formula are 0.96 and 0.97 respectively.

Fusion–fission cross-sections measured by the present formula along with experimental values for a few cases are given in table 2. First column of this table represents the compound nucleus and their fission fragments. Second column represents the energy (MeV). Third column represents the fusion–fission cross-section measured by the present formula and fourth column represents the corresponding experimental values. The references for the experimental values are given in the fifth column. This will repeat for different nuclei in the next five columns of this table.

The comparison of the fusion–fission cross-section measured by the present formulae for compound nuclei of atomic number range $23 \leq Z \leq 56$ is shown in figure 1. The values obtained by the present work agree well with the experiments. Similarly, the comparison of the fusion–fission cross-section measured by the present formulae for compound nuclei of atomic number range $57 \leq Z \leq 71$, $72 \leq Z \leq 88$, $89 \leq Z \leq 103$, and $104 \leq Z \leq 146$ in different energies are shown in figures 2–7. There may be up and down in the curves of plotted cross-sections because experiments show the results like that. This comparison also shows that the value produced by the present work agrees well with the experiments. We have also studied the variation of fusion–fission cross-section as a function of Z_1Z_2 at different energies such as 30, 50, 100, 150, 170, and 200 MeV. This variation is shown in figure 8. A symmetric/asymmetric system plays an important role in fusion–fission. At low excitation energy, shell effects play an important role and hence two fission modes, that is symmetric and asymmetric fission, comes into play. As excitation increases, asymmetric mode disappears and symmetric mode will be dominant [40].

The present formula is judged by evaluating the 'chi-square'. It is the measure of goodness of fit which is the ratio of the sum of the square of differences between experiment and theoretical frequencies.

$$\chi^2 = \sum_{i=1}^{N_{\mathrm{nucl}}} \frac{(\sigma_{\mathrm{th}}^i - \sigma_{\mathrm{exp}}^i)^2}{\sigma_{\mathrm{th}}^i}, \qquad (2)$$

Table 2. Fusion–fission cross-sections produced by the present formula along with experimental values are displayed for a few cases.

FF reaction	E (MeV)	FF cross-section (mb)		Reference	FF reaction	E (MeV)	FF cross-section (mb)		Reference
		Present work	Experiment				Present work	Experiment	
$^{20}Ne + {}^{50}Cr \rightarrow {}^{70}Se$	85.96	11.985	12.95439	[1]	$^{4}He + {}^{207}Pb \rightarrow {}^{211}Po$	76	180	197.831	[2]
$^{40}Ca + {}^{62}Ni \rightarrow {}^{102}Cd$	96.8	20	19.03438	[2]	$^{18}O + {}^{192}Os \rightarrow {}^{210}Po$	79.735	69.417	64.6218	[21]
$^{40}Ca + {}^{62}Ni \rightarrow {}^{102}Cd$	99.8	40	40.41122	[2]	$^{16}O + {}^{182}W \rightarrow {}^{198}Pb$	82.64	111.4	127.783	[2]
$^{40}Ca + {}^{62}Ni \rightarrow {}^{102}Cd$	99.9	40	41.02189	[2]	$^{6}Li + {}^{194}Pt \rightarrow {}^{200}Tl$	84.2	87.2	81.3342	[18]
$^{40}Ca + {}^{62}Ni \rightarrow {}^{102}Cd$	102.9	60	56.76169	[2]	$^{18}O + {}^{192}Os \rightarrow {}^{210}Po$	84.56	132.42	130.421	[21]
$^{35}Cl + {}^{62}Ni \rightarrow {}^{97}Rh$	105.2	90	82.00389	[2]	$^{12}C + {}^{198}Pt \rightarrow {}^{210}Po$	85	136	121.404	[2]
$^{20}Ne + {}^{92}Mo \rightarrow {}^{112}Te$	146	22	24.86322	[1]	$^{19}F + {}^{188}Os \rightarrow {}^{207}At$	85.175	143.4	132.096	[20]
$^{32}S + {}^{59}Co \rightarrow {}^{91}Tc$	178	342	381.3937	[2]	$^{19}F + {}^{181}Ta \rightarrow {}^{200}Pb$	86.754	121.37	130.407	[21]
$^{32}S + {}^{59}Co \rightarrow {}^{91}Tc$	198	387	389.4683	[2]	$^{16}O + {}^{186}W \rightarrow {}^{202}Pb$	87.45	125.9	127.329	[22]
$^{35}Cl + {}^{62}Ni \rightarrow {}^{97}Rh$	200	340	366.2249	[2]	$^{16}O + {}^{197}Au \rightarrow {}^{213}Fr$	87.7	141	130.205	[6]
$^{35}Cl + {}^{62}Ni \rightarrow {}^{97}Rh$	215	420	376.6353	[2]	$^{19}F + {}^{192}Os \rightarrow {}^{211}At$	89.037	115	131.878	[20]
$^{82}Kr + {}^{40}Ca \rightarrow {}^{122}Ba$	451	332	359.1921	[3]	$^{16}O + {}^{190}Os \rightarrow {}^{206}Po$	90	139	128.2	[2]
$^{18}O + {}^{150}Sm \rightarrow {}^{168}Yb$	103.99	17.319	15.58486	[4]	$^{19}F + {}^{181}Ta \rightarrow {}^{200}Pb$	90.364	221.71	253.998	[21]
$^{35}Cl + {}^{116}Sn \rightarrow {}^{151}Ho$	105.2	90	85.64005	[2]	$^{16}O + {}^{186}W \rightarrow {}^{202}Pb$	92.1	205.1	233.064	[22]
$^{16}O + {}^{141}Pr \rightarrow {}^{157}Ho$	108.5	7.7	7.884817	[6]	$^{19}F + {}^{192}Os \rightarrow {}^{211}At$	95.09	251.2	262.175	[20]
$^{12}C + {}^{158}Gd \rightarrow {}^{170}Yb$	124.2	31.9	28.01382	[5]	$^{19}F + {}^{197}Au \rightarrow {}^{216}Ra$	95.95	310.6	269.919	[2]
$^{12}C + {}^{158}Gd \rightarrow {}^{170}Yb$	126	16	15.79468	[7]	$^{16}O + {}^{184}W \rightarrow {}^{200}Pb$	97	228	227.617	[25]
$^{16}O + {}^{141}Pr \rightarrow {}^{157}Ho$	126.7	24.7	22.87196	[6]	$^{19}F + {}^{197}Au \rightarrow {}^{216}Ra$	99	273	268.049	[2]
$^{16}O + {}^{142}Nd \rightarrow {}^{158}Er$	130	21.6	23.45407	[2]	$^{16}O + {}^{192}Os \rightarrow {}^{208}Po$	100	270	235.133	[2]
$^{35}Cl + {}^{124}Sn \rightarrow {}^{159}Ho$	132.3	60	63.9899	[2]	$^{18}O + {}^{192}Os \rightarrow {}^{210}Po$	100	221	244.673	[2]
$^{16}O + {}^{141}Pr \rightarrow {}^{157}Ho$	143.2	73.5	83.43273	[6]	$^{19}F + {}^{181}Ta \rightarrow {}^{200}Pb$	101	215.3	245.78	[26]
$^{16}O + {}^{141}Pr \rightarrow {}^{157}Ho$	151.9	99.1	84.29869	[6]	$^{20}Ne + {}^{208}Pb \rightarrow {}^{228}U$	101.1	259.2	279.315	[2]
$^{34}S + {}^{238}U \rightarrow {}^{272}Hs$	157.9	64.84	58.00897	[2]	$^{19}F + {}^{181}Ta \rightarrow {}^{200}Pb$	101.2	219	245.628	[4]
$^{24}Mg + {}^{134}Ba \rightarrow {}^{158}Er$	160	188	192.1448	[2]	$^{20}Ne + {}^{208}Pb \rightarrow {}^{228}U$	102.5	305.1	278.603	[2]
$^{34}S + {}^{238}U \rightarrow {}^{272}Hs$	169.8	257	246.3375	[2]	$^{19}F + {}^{181}Ta \rightarrow {}^{200}Pb$	103.6	241	243.812	[25]
$^{16}O + {}^{142}Nd \rightarrow {}^{158}Er$	175	180	166.2275	[2]	$^{16}O + {}^{175}Lu \rightarrow {}^{191}Au$	103.7	233	205.511	[6]
$^{32}S + {}^{126}Te \rightarrow {}^{158}Er$	180	195	202.9324	[2]	$^{12}C + {}^{182}W \rightarrow {}^{194}Hg$	105.2	355.2	390.891	[9]
$^{40}Ar + {}^{116}Sn \rightarrow {}^{156}Er$	185.8	188.3	209.2061	[9]	$^{16}O + {}^{181}Ta \rightarrow {}^{197}Tl$	108	436	373.382	[23]
$^{35}Cl + {}^{116}Sn \rightarrow {}^{151}Ho$	200	500	471.3575	[2]	$^{16}O + {}^{175}Lu \rightarrow {}^{191}Au$	108.5	317	353.876	[6]
$^{32}S + {}^{126}Te \rightarrow {}^{158}Er$	220	445	490.7037	[2]	$^{28}Si + {}^{164}Er \rightarrow {}^{192}Pb$	111.27	151.17	157.107	[21]
$^{40}Ar + {}^{116}Sn \rightarrow {}^{156}Er$	220	406	437.3829	[2]	$^{28}Si + {}^{170}Er \rightarrow {}^{198}Pb$	112.22	150.04	148.68	[21]
$^{40}Ar + {}^{109}Ag \rightarrow {}^{149}Tb$	236	550	501.4637	[2]	$^{19}F + {}^{169}Tm \rightarrow {}^{188}Pt$	118	304	340.935	[4]
$^{40}Ar + {}^{116}Sn \rightarrow {}^{156}Er$	269.3	512.8	487.5284	[9]	$^{12}C + {}^{182}W \rightarrow {}^{194}Hg$	121	607	529.555	[27]

Table 2. *Continued.*

FF reaction	E (MeV)	FF cross-section (mb)		Reference	FF reaction	E (MeV)	FF cross-section (mb)		Reference
		Present work	Experiment				Present work	Experiment	
$^{40}Ar + {}^{116}Sn \rightarrow {}^{156}Er$	271	503	488.7115	[2]	$^{12}C + {}^{182}W \rightarrow {}^{194}Hg$	121	607	529.555	[2]
$^{40}Ar + {}^{109}Ag \rightarrow {}^{149}Tb$	288	600	522.4447	[2]	$^{30}Si + {}^{170}Er \rightarrow {}^{200}Pb$	121.29	203.32	226.394	[21]
$^{64}Ni + {}^{94}Zr \rightarrow {}^{158}Er$	290	420	358.8574	[2]	$^{30}Si + {}^{170}Er \rightarrow {}^{200}Pb$	122.99	252.65	231.567	[21]
$^{40}Ar + {}^{109}Ag \rightarrow {}^{149}Tb$	337	520	528.7018	[2]	$^{34}S + {}^{168}Er \rightarrow {}^{202}Po$	127	107	120.415	[2]
$^{32}S + {}^{126}Te \rightarrow {}^{158}Er$	350	520	529.1072	[2]	$^{34}S + {}^{168}Er \rightarrow {}^{202}Po$	127.83	124	123.533	[2]
$^{32}S + {}^{144}Nb \rightarrow {}^{176}La$	700	444	430.1873	[2]	$^{34}S + {}^{168}Er \rightarrow {}^{202}Po$	128.7	143	126.758	[2]
$^{6}He + {}^{209}Bi \rightarrow {}^{215}At$	31.5231	21.39	18.8187	[13]	$^{19}F + {}^{169}Tm \rightarrow {}^{188}Pt$	129	483	470.06	[4]
$^{6}He + {}^{209}Bi \rightarrow {}^{215}At$	33.7931	20.008	19.1047	[13]	$^{16}O + {}^{169}Tm \rightarrow {}^{185}Ir$	131.2	531	507.052	[6]
$^{7}Li + {}^{209}Bi \rightarrow {}^{216}Rn$	38.65	15.07	16.8426	[2]	$^{16}O + {}^{169}Tm \rightarrow {}^{185}Ir$	135.7	498	510.155	[6]
$^{6}Li + {}^{209}Bi \rightarrow {}^{215}Rn$	38.77	19.06	17.7609	[2]	$^{16}O + {}^{174}Yb \rightarrow {}^{190}Pt$	135.7	477	503.641	[6]
$^{6}Li + {}^{209}Bi \rightarrow {}^{215}Rn$	40	18.4	17.9243	[2]	$^{32}S + {}^{144}Sm \rightarrow {}^{176}Pt$	139.4	310	323.361	[2]
$^{7}Li + {}^{209}Bi \rightarrow {}^{216}Rn$	40	15	17.0529	[2]	$^{34}S + {}^{168}Er \rightarrow {}^{202}Po$	141.14	447	424.511	[2]
$^{11}Be + {}^{209}Bi \rightarrow {}^{220}Fr$	44.01	10.16	11.2915	[14]	$^{34}S + {}^{168}Er \rightarrow {}^{202}Po$	142.81	484	430.302	[2]
$^{11}Be + {}^{209}Bi \rightarrow {}^{220}Fr$	46.01	101.6	111.871	[14]	$^{40}Ar + {}^{165}Ho \rightarrow {}^{205}At$	151	353	312.512	[28]
$^{10}Be + {}^{209}Bi \rightarrow {}^{219}Fr$	49.59	132.3	118.061	[14]	$^{48}Ca + {}^{154}Sm \rightarrow {}^{202}Pb$	152.67	258	275.985	[2]
$^{11}Be + {}^{209}Bi \rightarrow {}^{220}Fr$	50	108	114.949	[14]	$^{4}He + {}^{238}U \rightarrow {}^{242}Pu$	23.37	191.49	168.1069	[39]
$^{11}B + {}^{238}U \rightarrow {}^{249}Bk$	50.41	99	96.7135	[2]	$^{4}He + {}^{238}U \rightarrow {}^{242}Pu$	24.02	228.57	203.6961	[37]
$^{32}S + {}^{150}Sm \rightarrow {}^{182}Pt$	159.1	624	629.654	[2]	$^{4}He + {}^{235}U \rightarrow {}^{239}Pu$	24.46	282	254.746	[2]
$^{32}S + {}^{152}Sm \rightarrow {}^{184}Pt$	159.5	614	626.509	[2]	$^{4}He + {}^{238}U \rightarrow {}^{242}Pu$	24.58	234.95	240.2778	[39]
$^{32}S + {}^{154}Sm \rightarrow {}^{186}Pt$	159.8	588	623.194	[2]	$^{4}He + {}^{233}U \rightarrow {}^{237}Pu$	24.96	326.38	315.5987	[37]
$^{22}Ne + {}^{159}Tb \rightarrow {}^{181}Re$	162.8	725	794.682	[6]	$^{4}He + {}^{233}U \rightarrow {}^{237}Pu$	27	600.06	581.5872	[37]
$^{16}O + {}^{169}Tm \rightarrow {}^{185}Ir$	166.1	774	835.002	[6]	$^{4}He + {}^{236}U \rightarrow {}^{240}Pu$	27	603	523.7983	[42]
$^{16}O + {}^{174}Yb \rightarrow {}^{190}Pt$	166.1	779	828.903	[6]	$^{4}He + {}^{233}U \rightarrow {}^{237}Pu$	27.28	678.1	632.3356	[39]
$^{32}S + {}^{144}Sm \rightarrow {}^{176}Pt$	166.2	684	653.195	[2]	$^{4}He + {}^{235}U \rightarrow {}^{239}Pu$	27.36	668	603.2781	[2]
$^{12}C + {}^{182}W \rightarrow {}^{194}Hg$	167	861	860.694	[2]	$^{4}He + {}^{238}U \rightarrow {}^{242}Pu$	27.43	629.72	554.8315	[39]
$^{22}Ne + {}^{159}Tb \rightarrow {}^{181}Re$	167.6	779	798.263	[6]	$^{4}He + {}^{233}U \rightarrow {}^{237}Pu$	27.5	628	675.27	[2]
$^{32}S + {}^{154}Sm \rightarrow {}^{186}Pt$	168.1	702	637.835	[2]	$^{4}He + {}^{236}U \rightarrow {}^{240}Pu$	28	673	703.463	[42]
$^{32}S + {}^{154}Sm \rightarrow {}^{186}Pt$	168.5	582.93	638.504	[30]	$^{4}He + {}^{238}U \rightarrow {}^{242}Pu$	28.7	770	804.0825	[15]
$^{64}Ni + {}^{118}Sn \rightarrow {}^{182}Po$	179.3	254.75	256.364	[31]	$^{4}He + {}^{238}U \rightarrow {}^{242}Pu$	30	1226.6	1174.242	[41]
$^{32}S + {}^{144}Sm \rightarrow {}^{176}Pt$	188.4	651.47	684.6	[30]	$^{4}He + {}^{238}U \rightarrow {}^{242}Pu$	31.23	979.55	1055.238	[39]
$^{22}Ne + {}^{159}Tb \rightarrow {}^{181}Re$	200	1020	1100.97	[6]	$^{4}He + {}^{233}U \rightarrow {}^{237}Pu$	31.36	1066.8	1070.307	[39]
$^{22}Ne + {}^{159}Tb \rightarrow {}^{181}Re$	205.9	1026	1103.32	[6]	$^{4}He + {}^{238}U \rightarrow {}^{242}Pu$	31.49	1016.3	1060.1	[39]
$^{22}Ne + {}^{159}Tb \rightarrow {}^{181}Re$	211.2	1147	1105.31	[6]	$^{4}He + {}^{233}U \rightarrow {}^{237}Pu$	31.73	1143.8	1077.092	[39]

$^{22}Ne + ^{159}Tb \rightarrow ^{181}Re$	218.2	1091	1107.8	[6]
$^{40}Ar + ^{164}Dy \rightarrow ^{204}Po$	221	852	863.824	[2]
$^{22}Ne + ^{159}Tb \rightarrow ^{181}Re$	223.3	1118	1109.51	[6]
$^{40}Ar + ^{165}Ho \rightarrow ^{205}Po$	226	800	856.587	[8]
$^{22}Ne + ^{159}Tb \rightarrow ^{181}Re$	228.4	1139	1111.15	[6]
$^{40}Ar + ^{165}Ho \rightarrow ^{205}At$	230	890	862.261	[34]
$^{20}Ne + ^{169}Tm \rightarrow ^{189}Au$	260	1210	1111.17	[29]
$^{40}Ar + ^{154}Sm \rightarrow ^{194}Hg$	272	919	975.483	[2]
$^{40}Ar + ^{164}Dy \rightarrow ^{204}Po$	272	949	923.634	[2]
$^{40}Ar + ^{154}Sm \rightarrow ^{194}Hg$	272.9	891.3	976.167	[9]
$^{20}Ne + ^{169}Tm \rightarrow ^{189}Au$	320	1160	1124.6	[29]
$^{56}Fe + ^{122}Sn \rightarrow ^{176}Os$	330	1050	981.291	[2]
$^{24}Mg + ^{181}Ta \rightarrow ^{205}At$	335	1090	1077.69	[34]
$^{24}Mg + ^{181}Ta \rightarrow ^{205}At$	340	1140	1079.23	[34]
$^{40}Ar + ^{154}Sm \rightarrow ^{194}Hg$	340.9	1040	1017.39	[9]
$^{56}Fe + ^{122}Sn \rightarrow ^{176}Os$	408	1070	1019.82	[2]
$^{56}Fe + ^{122}Sn \rightarrow ^{176}Os$	456	1030	1036.97	[2]
$^{4}He + ^{237}Np \rightarrow ^{241}Am$	22.7	133	114.7232	[2]
$^{4}He + ^{238}U \rightarrow ^{242}Pu$	22.72	142.64	138.6873	[39]
$^{132}Xe + ^{56}Fe \rightarrow ^{188}Hg$	1122	1040	1025.18	[36]
$^{4}He + ^{238}U \rightarrow ^{242}Pu$	21.58	95.138	98.88371	[37]
$^{4}He + ^{238}U \rightarrow ^{242}Pu$	21.6	93.9	99.47329	[38]
$^{4}He + ^{237}Np \rightarrow ^{241}Am$	22.3	101	102.2049	[2]
$^{4}He + ^{233}U \rightarrow ^{237}Pu$	22.32	144.61	142.3732	[40]
$^{4}He + ^{238}U \rightarrow ^{242}Pu$	22.83	153.28	143.2804	[41]
$^{4}He + ^{238}U \rightarrow ^{242}Pu$	22.9	162	146.2813	[15]
$^{19}F + ^{208}Pb \rightarrow ^{227}Pa$	86.7	158.61	150.2274	[52]
$^{19}F + ^{232}Th \rightarrow ^{251}Es$	87.51	57.575	64.00848	[53]
$^{12}C + ^{238}U \rightarrow ^{250}Cf$	90	1094	953.4563	[15]
$^{16}O + ^{208}Pb \rightarrow ^{224}Th$	91.45	479.4	519.2621	[2]
$^{12}C + ^{236}U \rightarrow ^{248}Cf$	95	1457	1287.836	[2]
$^{12}C + ^{238}U \rightarrow ^{250}Cf$	95	1235	1235.003	[2]
$^{16}O + ^{208}Pb \rightarrow ^{224}Th$	96	685	635.1683	[2]
$^{12}C + ^{238}U \rightarrow ^{250}Cf$	96.2	1311	1314.124	[15]
$^{16}O + ^{209}Bi \rightarrow ^{225}Pa$	99	620	613.3184	[6]
$^{238}U + ^{16}O \rightarrow ^{254}Fm$	101	730	790.6239	[2]
$^{14}N + ^{238}U \rightarrow ^{252}Es$	101.3	1057	1165.218	[15]
$^{14}N + ^{238}U \rightarrow ^{252}Es$	104	1200	1197.575	[15]
$^{12}C + ^{238}U \rightarrow ^{250}Cf$	104.5	1653	1574.979	[15]
$^{4}He + ^{238}U \rightarrow ^{242}Pu$	32	1041	1069.465	[15]
$^{4}He + ^{238}U \rightarrow ^{242}Pu$	32.01	1003.9	1069.647	[39]
$^{4}He + ^{233}U \rightarrow ^{237}Pu$	32.35	1157.2	1088.197	[39]
$^{4}He + ^{238}U \rightarrow ^{242}Pu$	32.41	1054.4	1076.833	[39]
$^{4}He + ^{233}U \rightarrow ^{237}Pu$	32.72	1212.2	1094.671	[39]
$^{4}He + ^{238}U \rightarrow ^{242}Pu$	32.73	1080.6	1082.487	[39]
$^{4}He + ^{238}U \rightarrow ^{242}Pu$	33.06	1107.5	1088.23	[39]
$^{4}He + ^{233}U \rightarrow ^{237}Pu$	33.5	1110	1107.96	[2]
$^{4}He + ^{238}U \rightarrow ^{242}Pu$	33.52	1135	1096.091	[39]
$^{4}He + ^{233}U \rightarrow ^{237}Pu$	33.59	1255.2	1109.463	[39]
$^{4}He + ^{235}U \rightarrow ^{239}Pu$	33.8	1030	1108.071	[43]
$^{4}He + ^{238}U \rightarrow ^{242}Pu$	33.8	970	1100.796	[44]
$^{4}He + ^{238}U \rightarrow ^{242}Pu$	33.98	1163.2	1103.79	[39]
$^{4}He + ^{238}U \rightarrow ^{242}Pu$	34.4	1163	1110.68	[15]
$^{4}He + ^{233}U \rightarrow ^{237}Pu$	34.5	1090	1124.316	[44]
$^{7}Li + ^{235}U \rightarrow ^{242}Am$	34.95	463.5	480.4559	[2]
$^{4}He + ^{238}U \rightarrow ^{242}Pu$	34.96	1206.8	1119.668	[39]
$^{4}He + ^{238}U \rightarrow ^{242}Pu$	35.48	1252.1	1127.817	[39]
$^{4}He + ^{238}U \rightarrow ^{242}Pu$	36.53	1299	1143.716	[39]
$^{6}Li + ^{235}U \rightarrow ^{241}Am$	37.05	623.7	624.3188	[2]
$^{4}He + ^{238}U \rightarrow ^{242}Pu$	37.1	591.8	616.451	[39]
$^{4}He + ^{238}U \rightarrow ^{242}Pu$	39.9	1317	1190.216	[44]
$^{4}He + ^{233}U \rightarrow ^{237}Pu$	40.5	1345	1208.777	[44]
$^{3}He + ^{232}Th \rightarrow ^{235}U$	44.49	1249.1	1408.355	[2]
$^{11}B + ^{232}Th \rightarrow ^{243}Am$	61.04	722.8	661.9303	[2]
$^{16}O + ^{204}Pb \rightarrow ^{220}Th$	79.407	219.495	227.6735	[50]
$^{16}O + ^{208}Pb \rightarrow ^{224}Th$	79.72	208.23	186.9287	[2]
$^{13}C + ^{232}Th \rightarrow ^{245}Cm$	62.98	153.31	167.13	[2]
$^{15}N + ^{209}Bi \rightarrow ^{224}Th$	72.66	307.49	301.618	[2]
$^{12}C + ^{232}Th \rightarrow ^{244}Cm$	73.98	458.72	422.9289	[50]
$^{18}O + ^{208}Pb \rightarrow ^{226}Th$	77.12	141.37	128.707	[2]
$^{11}B + ^{237}Np \rightarrow ^{248}Cf$	80	1388	1466.882	[2]
$^{28}Si + ^{208}Pb \rightarrow ^{236}Cm$	153.3	657.79	627.0118	[59]
$^{29}Al + ^{197}Au \rightarrow ^{226}U$	154.2	1000	893.2365	[2]
$^{31}Al + ^{197}Au \rightarrow ^{228}U$	154.2	841.7	812.2767	[54]
$^{28}Si + ^{208}Pb \rightarrow ^{236}Cm$	155	696.19	639.9732	[59]
$^{32}S + ^{208}Pb \rightarrow ^{240}Cf$	155.8	279.26	314.2475	[2]
$^{28}Si + ^{208}Pb \rightarrow ^{236}Cm$	156.8	728.7	653.5951	[2]
$^{32}S + ^{208}Pb \rightarrow ^{240}Cf$	157.7	308.39	325.5251	[2]

Table 2. *Continued.*

FF reaction	E (MeV)	FF cross-section (mb)		Reference	FF reaction	E (MeV)	FF cross-section (mb)		Reference
		Present work	Experiment				Present work	Experiment	
$^{14}N + ^{238}U \rightarrow ^{252}Es$	107.9	1254	1242.281	[15]	$^{38}S + ^{181}Ta \rightarrow ^{219}Ac$	158	626.91	624.4677	[60]
$^{16}O + ^{238}U \rightarrow ^{254}Fm$	108.4	848.2	883.7892	[15]	$^{34}S + ^{204}Pb \rightarrow ^{238}Cf$	158.0	320.6	290.0149	[2]
$^{12}C + ^{238}U \rightarrow ^{248}Cf$	110	1800	1635.302	[2]	$^{34}S + ^{206}Pb \rightarrow ^{240}Cf$	158.2	296.9	282.3549	[2]
$^{12}C + ^{238}U \rightarrow ^{250}Cf$	110.6	1758	1632.284	[2]	$^{32}S + ^{208}Pb \rightarrow ^{240}Cf$	159.4	332.95	335.6585	[2]
$^{16}O + ^{238}U \rightarrow ^{254}Fm$	111	971.5	914.8435	[15]	$^{40}Ar + ^{181}Ta \rightarrow ^{221}Pa$	160	379	401.3848	[2]
$^{14}N + ^{238}U \rightarrow ^{252}Es$	112.4	1420	1291.066	[15]	$^{29}Al + ^{197}Au \rightarrow ^{226}U$	160.3	1000	940.1631	[54]
$^{14}N + ^{238}U \rightarrow ^{252}Es$	115.8	1500	1326.07	[15]	$^{32}S + ^{208}Pb \rightarrow ^{240}Cf$	160.3	365.5	341.0372	[2]
$^{12}C + ^{238}U \rightarrow ^{250}Cf$	117.8	1858	1693.579	[15]	$^{40}Ar + ^{197}Au \rightarrow ^{237}Bk$	162	155	166.6239	[61]
$^{12}C + ^{238}U \rightarrow ^{250}Cf$	117.8	1915	1693.579	[15]	$^{40}Ar + ^{180}Hf \rightarrow ^{220}Th$	164	519	471.426	[28]
$^{11}B + ^{237}Np \rightarrow ^{258}Cf$	118	2023	1923.653	[2]	$^{40}Ar + ^{179}Hf \rightarrow ^{219}Th$	165	431	484.1769	[28]
$^{16}O + ^{232}Th \rightarrow ^{248}Cf$	120	1150	1127.642	[2]	$^{40}Ar + ^{209}Bi \rightarrow ^{249}Md$	167	92	94.90762	[62]
$^{208}Pb + ^{26}Mg \rightarrow ^{234}Pu$	121	360.55	358.773	[55]	$^{40}Ar + ^{175}Lu \rightarrow ^{215}Ac$	169	534	577.6383	[28]
$^{23}Na + ^{206}Pb \rightarrow ^{229}Np$	121.9	633.99	672.8942	[56]	$^{19}F + ^{208}Pb \rightarrow ^{227}Pa$	170	1615	1767.052	[28]
$^{12}C + ^{238}U \rightarrow ^{250}Cf$	122	1707	1726.531	[2]	$^{32}S + ^{182}W \rightarrow ^{214}Th$	170.2	853.9	870.4967	[2]
$^{19}F + ^{208}Pb \rightarrow ^{227}Pa$	123.9	1231.6	1241.581	[52]	$^{40}Ar + ^{176}Hf \rightarrow ^{216}Th$	171	560	543.0011	[28]
$^{19}F + ^{209}Bi \rightarrow ^{228}U$	125.6	1109	1211.084	[57]	$^{40}Ar + ^{177}Hf \rightarrow ^{217}Th$	171	531	536.5638	[28]
$^{12}C + ^{238}U \rightarrow ^{248}Cf$	130	1948	1791.809	[2]	$^{40}Ar + ^{178}Hf \rightarrow ^{218}Th$	171	569	530.1835	[28]
$^{30}Si + ^{206}Au \rightarrow ^{236}Cm$	130.7	131.1	137.3067	[2]	$^{40}Ar + ^{179}Hf \rightarrow ^{219}Th$	171	579	523.8598	[28]
$^{28}Si + ^{208}Pb \rightarrow ^{236}Cm$	133.8	190.01	177.6258	[59]	$^{40}Ar + ^{189}Hf \rightarrow ^{220}Th$	171	574	517.5926	[28]
$^{19}F + ^{209}Pb \rightarrow ^{227}Pa$	135	1245	1342.989	[15]	$^{16}O + ^{238}U \rightarrow ^{254}Fm$	175	1775	1660.406	[2]
$^{28}Si + ^{198}Pt \rightarrow ^{226}U$	140	456	430.9472	[2]	$^{38}S + ^{181}Ta \rightarrow ^{219}Ac$	176.2	705.14	754.2842	[60]
$^{4}He + ^{233}U \rightarrow ^{237}Pu$	140	2490	2703.089	[2]	$^{40}Ca + ^{192}Os \rightarrow ^{232}Cm$	177.6	200.02	215.3569	[2]
$^{34}S + ^{208}Pb \rightarrow ^{242}Cf$	140.59	13.45	14.36765	[2]	$^{40}Ca + ^{192}Os \rightarrow ^{232}Cm$	177.7	210.48	215.7753	[63]
$^{36}S + ^{204}Pb \rightarrow ^{240}Cf$	141	20.308	18.13877	[2]	$^{40}Ca + ^{192}Os \rightarrow ^{232}Cm$	178.5	212.99	219.1333	[2]
$^{32}S + ^{208}Pb \rightarrow ^{240}Cf$	141.2	20.038	20.82297	[2]	$^{40}Ca + ^{192}Os \rightarrow ^{232}Cm$	178.6	218.66	219.5544	[63]
$^{27}Al + ^{197}Au \rightarrow ^{224}U$	143.7	525.19	594.9111	[54]	$^{40}Ca + ^{192}Os \rightarrow ^{232}Cm$	179.6	228.66	223.7813	[2]
$^{32}O + ^{208}Pb \rightarrow ^{224}Th$	148	1770	1760.842	[2]	$^{40}Ca + ^{192}Os \rightarrow ^{232}Cm$	179.7	240.56	224.2056	[63]
$^{20}Ne + ^{209}Bi \rightarrow ^{229}Np$	148	1200	1193.585	[2]	$^{28}Si + ^{208}Pb \rightarrow ^{232}Cm$	180	740	819.1718	[2]
$^{32}S + ^{182}W \rightarrow ^{214}Th$	149.6	419.6	406.6187	[2]	$^{40}Ca + ^{192}Os \rightarrow ^{232}Cm$	180.9	254.35	229.3185	[2]
$^{27}Al + ^{197}Au \rightarrow ^{224}U$	149.9	721.96	650.1525	[54]	$^{40}Ca + ^{194}Pt \rightarrow ^{234}Cf$	181.4	157.8	176.2537	[2]
$^{19}F + ^{208}Pb \rightarrow ^{227}Pa$	150	1440	1461.707	[2]	$^{40}Ca + ^{194}Pt \rightarrow ^{234}Cf$	181.4	156.82	176.2537	[63]
$^{208}Pb + ^{26}Mg \rightarrow ^{234}Pu$	150	956	925.9939	[2]	$^{40}Ca + ^{194}Pt \rightarrow ^{234}Cf$	182.4	173.34	179.8085	[2]
$^{208}Pb + ^{26}Mg \rightarrow ^{234}Pu$	150.3	967.13	928.4092	[55]	$^{40}Ca + ^{194}Pt \rightarrow ^{234}Cf$	182.5	175.82	180.166	[63]
$^{36}S + ^{204}Pb \rightarrow ^{240}Cf$	150.3	209.59	203.5285	[2]	$^{38}S + ^{181}Ta \rightarrow ^{219}Ac$	182.7	810	798.0185	[2]
$^{36}S + ^{204}Pb \rightarrow ^{240}Cf$	151.2	226.4	207.8261	[2]	$^{40}Ca + ^{194}Pt \rightarrow ^{234}Cf$	183.5	187.88	183.7608	[2]

$^{23}Na + ^{206}Pb \rightarrow ^{229}Np$	152.1	1276.2	1227.059	[56]	$^{40}Ca + ^{194}Pt \rightarrow ^{234}Cf$	183.6	189.75	184.1222	[63]
$^{208}Pb + ^{26}Mg \rightarrow ^{234}Pu$	185	1300	1175.143	[58]	$^{32}S + ^{181}Ta \rightarrow ^{213}Ac$	184.3	909.8	1016.552	[63]
$^{208}Pb + ^{26}Mg \rightarrow ^{234}Pu$	186.3	1327.6	1183.241	[55]	$^{40}Ca + ^{194}Pt \rightarrow ^{234}Cf$	184.7	209.16	188.1207	[2]
$^{19}F + ^{208}Pb \rightarrow ^{227}Pa$	190	1910	1858.698	[2]	$^{40}Ca + ^{194}Pt \rightarrow ^{234}Cf$	184.8	212.74	188.4862	[63]
$^{24}Mg + ^{208}Pb \rightarrow ^{232}Pu$	190	1345	1296.624	[2]	$^{56}Fe + ^{165}Ho \rightarrow ^{221}Np$	261.7	642.18	622.2025	[2]
$^{38}S + ^{181}Ta \rightarrow ^{219}Ac$	190.5	950	848.6412	[2]	$^{32}S + ^{181}Ta \rightarrow ^{213}Ac$	265.5	1090	1209.903	[2]
$^{38}S + ^{181}Ta \rightarrow ^{219}Ac$	195.5	941.25	880.0341	[60]	$^{32}S + ^{181}Ta \rightarrow ^{213}Ac$	274.3	1150	1229.661	[2]
$^{28}Si + ^{208}Pb \rightarrow ^{232}Cm$	200	990	946.7173	[2]	$^{12}C + ^{238}U \rightarrow ^{240}Cf$	291	2050	2032.519	[2]
$^{32}S + ^{181}Ta \rightarrow ^{213}Ac$	204.7	1013.6	1052.317	[60]	$^{48}Ca + ^{208}Pb \rightarrow ^{256}No$	300	600	582.4686	[69]
$^{40}Ca + ^{208}Pb \rightarrow ^{258}No$	207.92	494	470.9473	[2]	$^{48}Ca + ^{208}Pb \rightarrow ^{256}No$	300	600	582.4686	[69]
$^{38}S + ^{181}Ta \rightarrow ^{219}Ac$	210.5	999.44	964.9085	[60]	$^{40}Ca + ^{197}Au \rightarrow ^{237}Es$	310.7	1215	1280.503	[2]
$^{38}S + ^{181}Ta \rightarrow ^{219}Ac$	211.9	988.39	968.9252	[60]	$^{56}Fe + ^{165}Ho \rightarrow ^{221}Np$	313.6	820.31	731.8282	[2]
$^{32}S + ^{181}Ta \rightarrow ^{213}Ac$	213.8	1041.3	1078.673	[60]	$^{16}O + ^{238}U \rightarrow ^{254}Fm$	315	1825	1706.716	[2]
$^{16}O + ^{208}Pb \rightarrow ^{224}Th$	215	1916	1754.707	[65]	$^{60}Ni + ^{154}Sm \rightarrow ^{214}Th$	339	900	820.8797	[2]
$^{32}S + ^{181}Ta \rightarrow ^{213}Ac$	215.6	1000	1083.753	[2]	$^{56}Fe + ^{165}Ho \rightarrow ^{221}Np$	344.9	723.43	789.4747	[2]
$^{32}S + ^{197}Au \rightarrow ^{229}Am$	219	830	914.82	[2]	$^{14}N + ^{232}Th \rightarrow ^{246}Bk$	742	2780	2453.764	[35]
$^{32}S + ^{182}W \rightarrow ^{214}Th$	222	945	1076.344	[2]	$^{16}O + ^{248}Cm \rightarrow ^{264}Rf$	110	850	943.2723	[2]
$^{32}S + ^{181}Ta \rightarrow ^{213}Ac$	225.3	1040	1110.419	[2]	$^{238}U + ^{27}Al \rightarrow ^{265}Db$	146	405	463.0873	[74]
$^{32}S + ^{181}Ta \rightarrow ^{213}Ac$	226	1099.1	1112.299	[60]	$^{30}Si + ^{238}U \rightarrow ^{268}Sg$	148.9	397.9	351.9963	[75]
$^{32}S + ^{208}Pb \rightarrow ^{240}Cf$	230	866	851.2326	[2]	$^{30}Si + ^{238}U \rightarrow ^{268}Sg$	154	396.5	371.6981	[2]
$^{32}S + ^{181}Ta \rightarrow ^{213}Ac$	239.6	1030	1147.707	[2]	$^{238}U + ^{27}Al \rightarrow ^{264}Db$	182	560	616.3141	[2]
$^{48}Ca + ^{208}Pb \rightarrow ^{256}No$	242	480	452.2863	[66]	$^{32}S + ^{238}U \rightarrow ^{274}Hs$	199	429	384.1905	[2]
$^{12}C + ^{238}U \rightarrow ^{240}Cf$	245	1970	1928.259	[2]	$^{50}Ti + ^{208}Pb \rightarrow ^{264}Rf$	210	204	191.4284	[28]
$^{32}S + ^{181}Ta \rightarrow ^{213}Ac$	245.9	1129.2	1163.434	[60]	$^{50}Ti + ^{209}Bi \rightarrow ^{265}Db$	210	175	178.0118	[28]
$^{40}Ar + ^{197}Au \rightarrow ^{237}Bk$	248	810	758.1028	[67]	$^{208}Pb + ^{52}Pb \rightarrow ^{260}Sg$	245	210	187.541	[58]
$^{32}S + ^{208}Pb \rightarrow ^{240}Cf$	250	975	901.7566	[2]	$^{208}Pb + ^{52}Pb \rightarrow ^{260}Sg$	245.5	198.96	188.3107	[55]
$^{32}S + ^{208}Pb \rightarrow ^{240}Cf$	250	968	901.7566	[2]	$^{58}Ti + ^{208}Pb \rightarrow ^{266}Hs$	266.1	132.7	139.6654	[55]
$^{32}S + ^{181}Ta \rightarrow ^{213}Ac$	250.6	1130	1174.906	[2]	$^{58}Ti + ^{208}Pb \rightarrow ^{266}Hs$	268	135	141.7302	[58]
$^{20}Ne + ^{238}U \rightarrow ^{258}No$	252	1360	1284.399	[15]	$^{32}S + ^{238}U \rightarrow ^{274}Hs$	700	1265	1265.046	[2]
$^{32}S + ^{182}W \rightarrow ^{214}Th$	260	1225	1172.084	[2]	$^{56}Fe + ^{165}Ho \rightarrow ^{221}Np$	261.7	642.18	622.2025	[2]

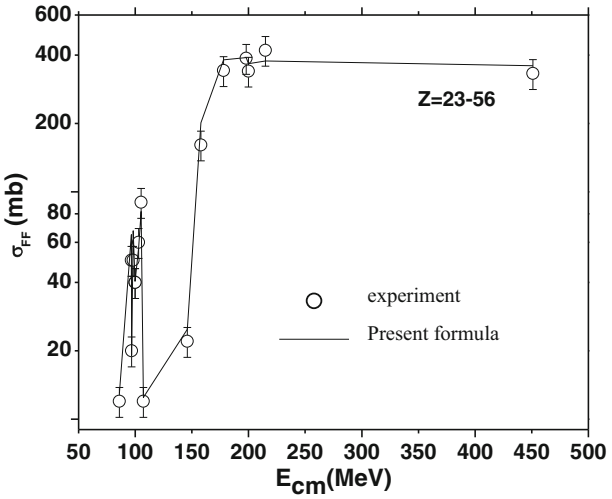

Figure 1. The comparison of fusion–fission cross-section measured by the present formulae for compound nuclei of atomic number range $23 \leq Z \leq 56$.

where N_{nucl} represents the number of nuclei considered in the fitting procedure. σ^i_{th} and σ^i_{exp} are cross-sections measured by the present formula and their corresponding experimental values. The present formula is judged by calculating the coefficient of determination (R^2). It is the ratio of theoretical variation to the experimental variation and is expressed as

$$R^2 = 1 - \frac{\text{SS}_{\text{Res}}}{\text{SS}_{\text{Res}} + \text{SS}_{\text{Reg}}} \tag{3}$$

The second term in the equation is the fraction of variance unexplained (FVU). SS_{Res} is the sum of the squares of the residuals and SS_{Reg} is the regression sum of the squares. The calculated χ^2 and R^2 for the present formula are given in table 3.

The agreement of the present work with the experiment may lead to the conclusion that these formulae may be used to obtain fusion–fission cross-section of compound nuclei of atomic number range $23 \leq Z \leq 146$. Our analytical parametrised values are in very close agreement with actual as well as experimental values. Our parametrisations depend on the charges and masses of the compound nuclei and fission fragments only. This definitely introduces great simplification in the calculation of fusion–fission cross-sections. These results can be used as a guideline for estimating the fusion–fission cross-sections in those cases where measurements do not exist and also for studying new unexplored nuclei.

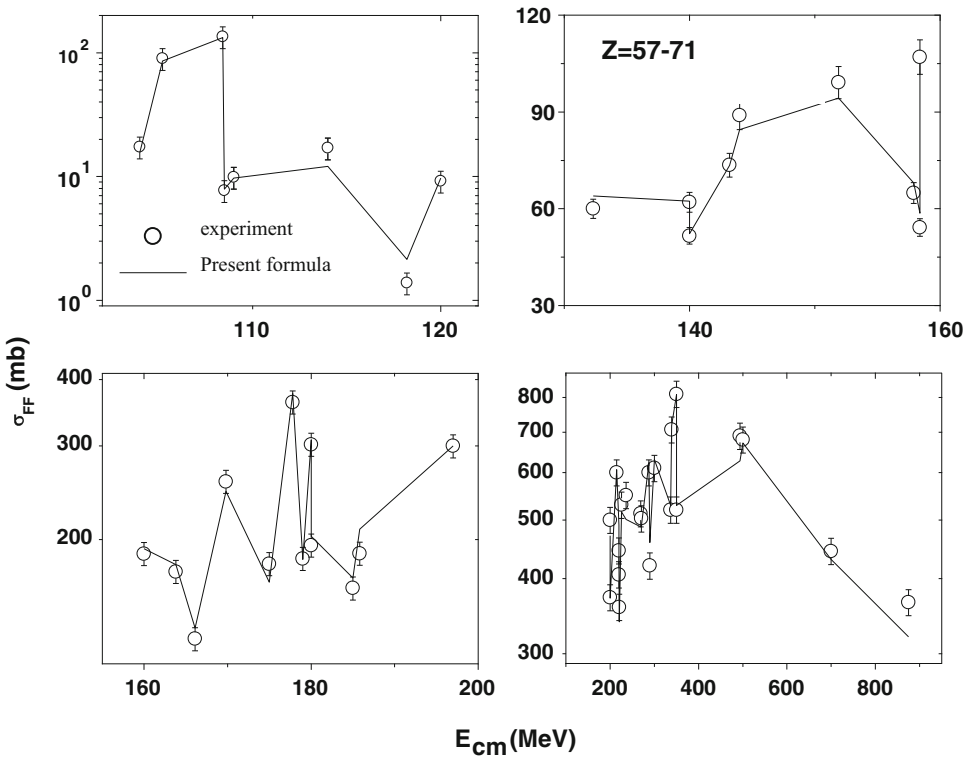

Figure 2. The comparison of fusion–fission cross-section measured by the present formulae for compound nuclei of atomic number range $57 \leq Z \leq 71$.

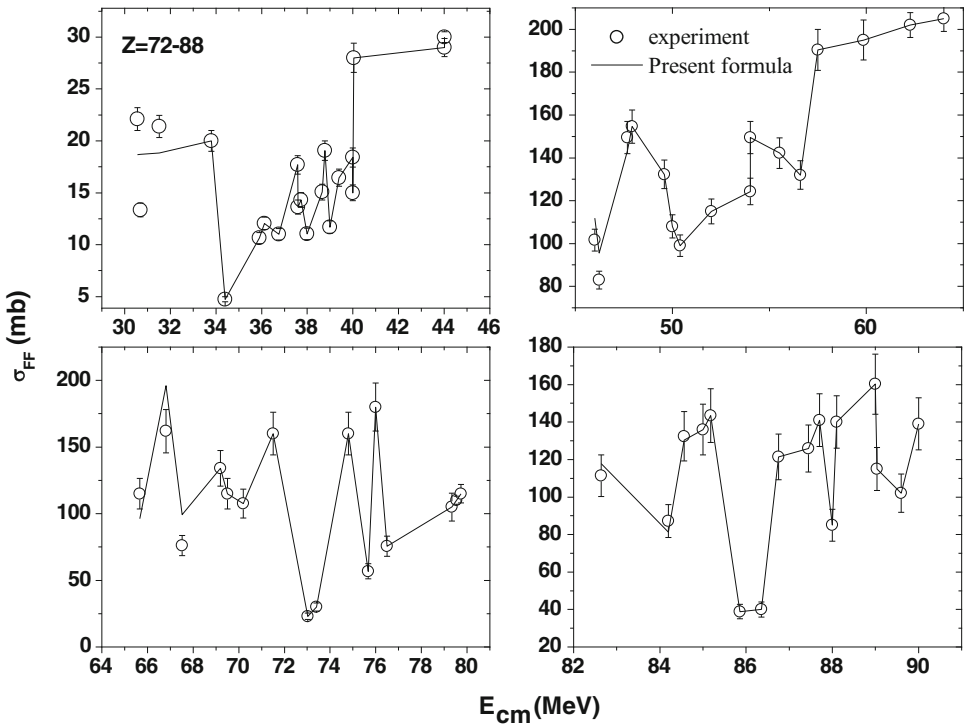

Figure 3. The comparison of fusion–fission cross-section measured by the present formulae for compound nuclei of atomic number range $72 \leq Z \leq 88$ in the energy range 0–90 MeV.

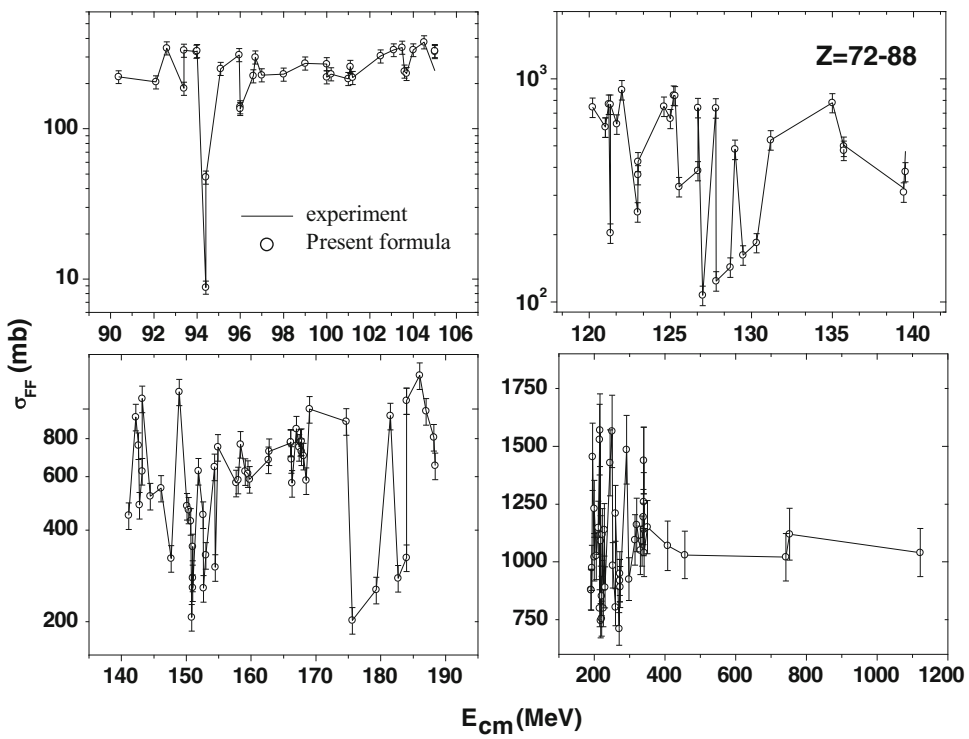

Figure 4. The comparison of fusion–fission cross-section measured by the present formulae for compound nuclei of atomic number range $72 \leq Z \leq 88$ in the energy range 90–500 MeV.

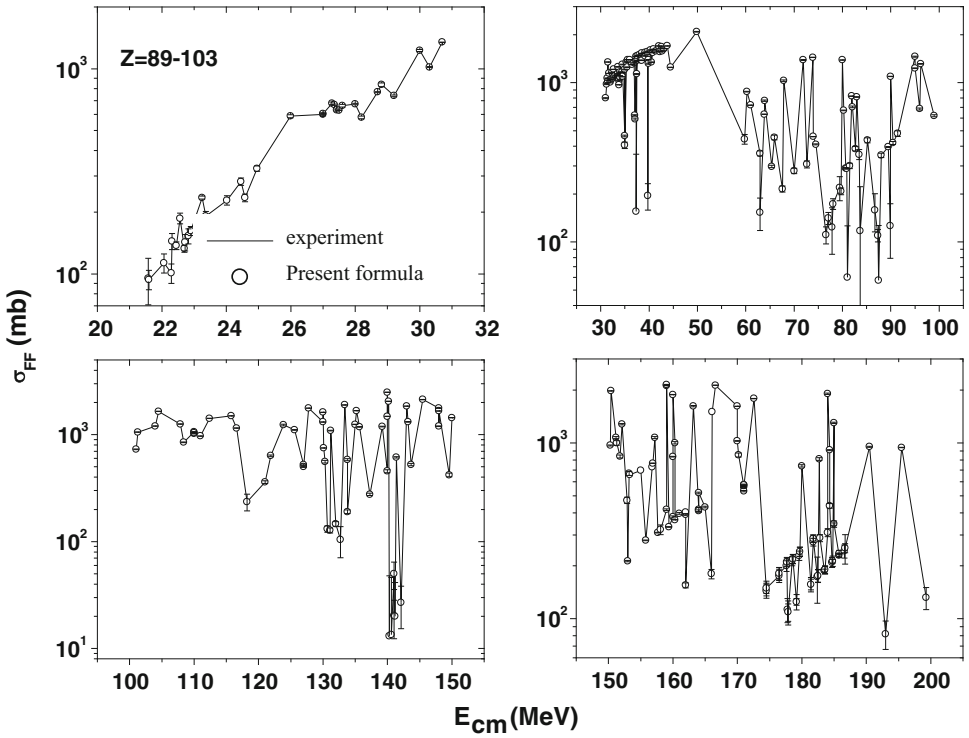

Figure 5. The comparison of fusion–fission cross-section measured by the present formulae for compound nuclei of atomic number range $89 \leq Z \leq 103$ in the energy range up to 200 MeV.

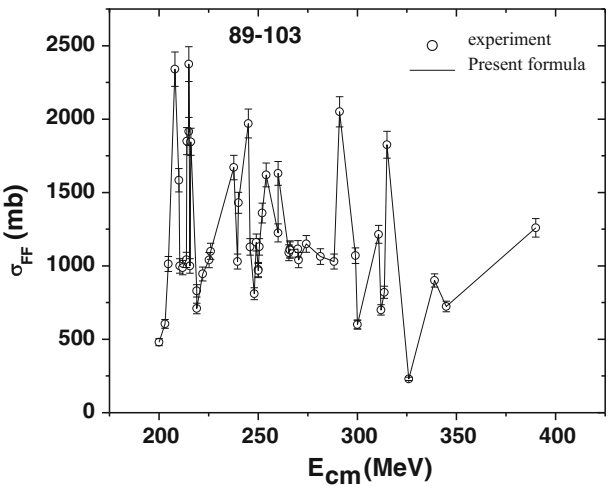

Figure 6. The comparison of fusion–fission cross-section measured by the present formulae for compound nuclei of atomic number range $89 \leq Z \leq 103$ in the energy range up to 400 MeV.

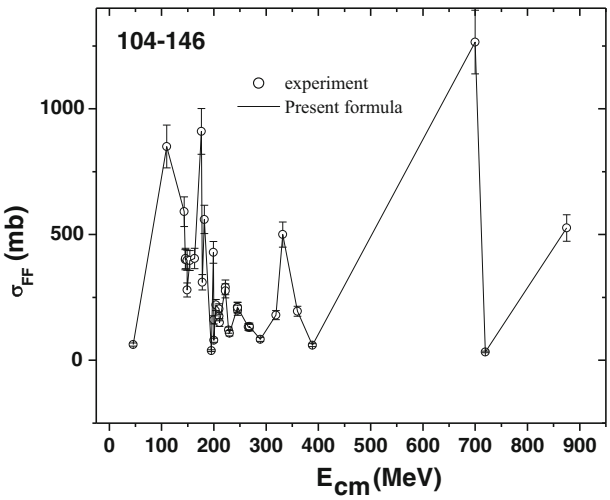

Figure 7. The comparison of fusion–fission cross-section measured by the present formulae for compound nuclei of atomic number range $104 \leq Z \leq 146$ in the energy range up to 1000 MeV.

4. Conclusion

In summary, the present parametrisation of the fusion–fission cross-sections allows us to estimate values of these cross-sections with very good accuracy. Therefore, parametrisation can be applied for interpolation and/or extrapolation of the present experimental information on fusion–fission cross-sections to the fission fragment or energies not available experimentally.

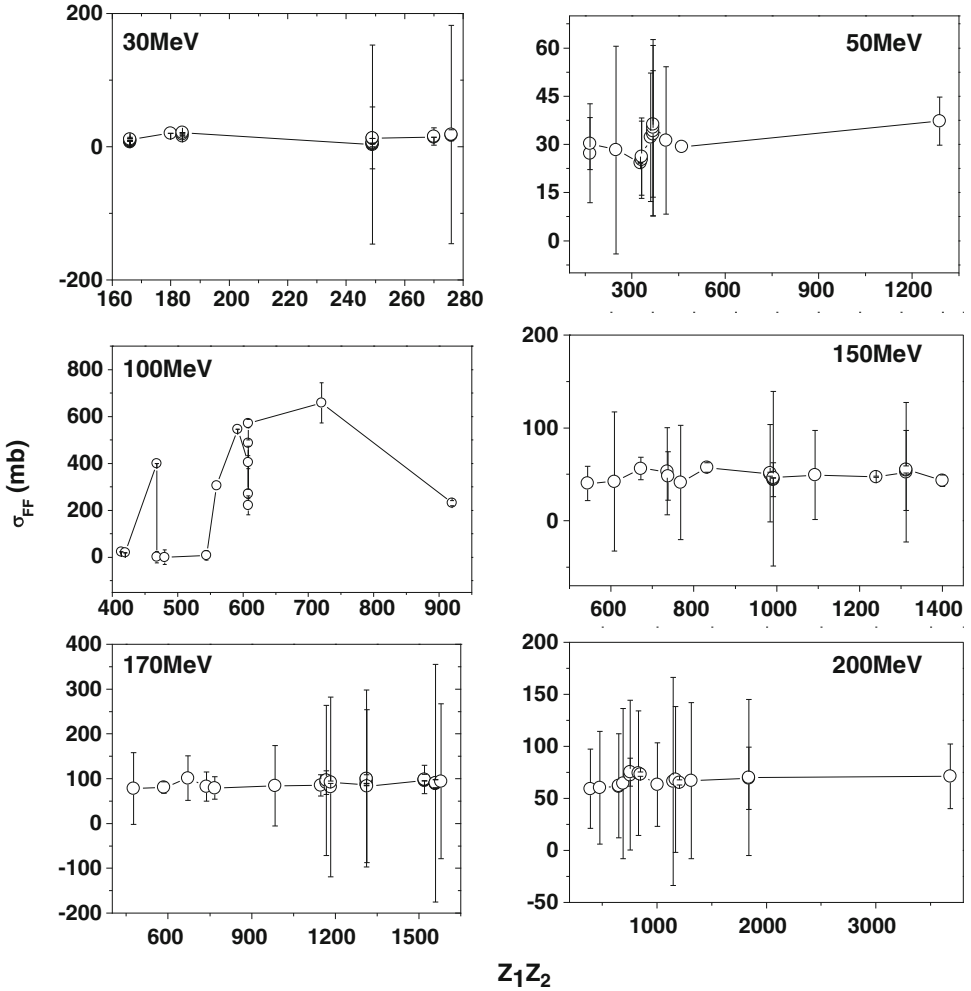

Figure 8. The variation of fusion–fission cross-section as a function of Z_1Z_2 at different energies.

Table 3. Chi-square (χ^2) and coefficient of determination R^2 of the present formula for different atomic number ranges.

Region	χ^2	R^2
$23 \leq Z \leq 56$	2.21	0.96
$57 \leq Z \leq 71$	10.73	0.95
$72 \leq Z \leq 88$	19.72	0.96
$89 \leq Z \leq 103$	40.37	0.95
$104 \leq Z \leq 146$	19.09	0.96

References

[1] Y Nagame *et al*, *Z. Phys. A* **31**, 317 (1984)
[2] http://nrv.jinr.ru/nrv/webnrv/fusion/reactions.php
[3] G Ademard *et al*, *Phys. Rev. C* **83**, 54619 (2011)
[4] R J Charity *et al*, *Nucl. Phys. A* **457**, 441 (1986)
[5] F Plasil *et al*, *Phys. Rev. Lett*. **45**, 333 (1980)
[6] Torbjorn Sikkeland, *Phys. Rev*. **135**, 669 (1964)
[7] A M Zebelman and J M Miller, *Phys. Rev. Lett*. **30**, 27 (1973)
[8] B Tamain *et al*, *Nucl. Phys. A* **252**, 187 (1975)
[9] H Delagrange *et al*, *Phys. Rev. Lett*. **43**, 1490 (1979)
[10] R A Esterlund *et al*, *Nucl. Phys. A* **435**, 597 (1985)
[11] J R Huizenga, R Chaudhry and R Vandenbosch, *Phys. Rev*. **126**, 210 (1962)
[12] A S Fomichev *et al*, *Z. Phys*. **351**, 129 (1995)
[13] Yu E Penionzhkevich *et al*, *Eur. Phys. J. A* **13**, 123 (2002)
[14] C Signorini *et al*, *Nucl. Phys. A* **735**, 329 (2004)
[15] Victor E Viola, *Phys. Rev*. **128**, 767 (1962)
[16] Kushal Kalita, *J. Phys. G* **38**, 95104 (2011)
[17] A Shrivastava *et al*, *Phys. Rev. Lett*. **82**, 699 (1999)
[18] S E Vigdor *et al*, *Phys. Rev. C* **26**, 1035 (1982)
[19] P V Laveen *et al*, *J. Phys. G* **42**, 95105 (2015)
[20] K Mahata *et al*, *Nucl. Phys. A* **720**, 209(2003)
[21] D J Hinde *et al*, *Nucl. Phys. A* **452**, 550 (1986)
[22] M Trotta *et al*, *Eur. Phys. J. A* **25**, 615 (2005)
[23] Bivash R Behera *et al*, *Pramana – J. Phys*. **57**, 199 (2001)
[24] K Mahata *et al*, *Phys. Rev. C* **65**, 34613 (2002)
[25] J S Forster *et al*, *Nucl. Phy. A* **464**, 497 (1987)
[26] D J Hinde *et al*, *Nucl. Phys. A* **385**, 109 (1982)
[27] J M Miller *et al*, *Phys. Rev. Lett*. **40**, 1074 (1978)
[28] H G Clerc *et al*, *Nucl. Phys. A* **419**, 571 (1984)

[29] J Cabrera *et al*, *Phys. Rev. C* **68**, 034613 (2003)
[30] B B Back *et al*, *Phys. Rev. Lett*. **45**, 1230 (1980)
[31] K T Lesko *et al*, *Phys. Rev. Lett*. **55**, 803 (1985)
[32] F L H Wolfs *et al*, *Phys. Lett. B* **196**, 113 (1987)
[33] Z Kohley *et al*, *Phys. Rev. Lett*. **107**, 202701 (2011)
[34] B Borderie *et al*, *Z. Phys. A* **299**, 263 (1981)
[35] C M Herbach *et al*, *Nucl. Phys. A* **712**, 207(2002)
[36] D Bangert *et al*, *Nucl. Phys. A* **456**, 489 (1986)
[37] H Freiesleben and J R Huizenga, *Nucl. Phys. A* **224**, 503 (1974)
[38] M Trotta *et al*, *Phys. Rev. Lett*. **84**, 2342 (2000)
[39] J R Huizenga, R Vandenbosch and H Warhanek, *Phys. Rev*. **124**, 1964 (1961)
[40] T K Ghosh *et al*, *Pramana – J. Phys*. **85**, 2 (2015)
[41] R Raabe *et al*, *Nature* **431**, 823 (2004)
[42] P Limkilde and G Sletten, *Nucl. Phys. A* **199**, 504 (1973)
[43] R Gunnink and J W Cobble, *Phys. Rev*. **115**, 1247 (1959)
[44] L J Colby Jr, Mary Shoaf and J W Cobble, *Phys. Rev*. **121**, 1415 (1961)
[45] V Fekou-Youmbi *et al*, *J. Phys. G* **23**, 1259 (1997)
[46] V Fekou-Youmbi *et al*, *Nucl. Phys. A* **583**, 811 (1995)
[47] V S Ramamurthy *et al*, *Phys. Rev. Lett*. **65**, 25 (1990)
[48] R Tripathi *et al*, *Phys. Rev. C* **75**, 024609 (2007)
[49] A Karnik *et al*, *Z. Phys*. **351**, 195 (1995)
[50] M Dasgupta *et al*, *Phys. Rev. Lett*. **99**, 192701 (2007)
[51] K E Rehm *et al*, *Phys. Rev. Lett*. **81**, 3341 (1998)
[52] Zhang Huanqiao *et al*, *Nucl. Phys. A* **512**, 531 (1990)
[53] Huanqiao Zhang *et al*, *Phys. Lett. B* **218**, 133 (1989)
[54] Y X Watanabe *et al*, *Eur. Phys. J. A* **10**, 373 (2001)
[55] H Sann *et al*, *Phys. Rev. Lett*. **47**, 1248 (1981)
[56] H Reich *et al*, *Nucl. Phys. A* **576**, 409 (1994)
[57] A M Samant *et al*, *Eur. Phys. J. A* **7**, 59 (2000)
[58] R Bock *et al*, *Nucl. Phys. A* **388**, 334 (1982)
[59] D J Hinde *et al*, *Nucl. Phys. A* **592**, 271 (1995)
[60] W Loveland *et al*, *J. Phys. G* **23**, 1251 (1997)
[61] C Ngo *et al*, *Z. Phys*. **283**, 161 (1977)
[62] M F Rivet *et al*, *Z. Phys*. **330**, 395 (1988)
[63] J D Bierman *et al*, *Phys. Rev. Lett*. **76**, 1587 (1996)
[64] V E Viola Jr *et al*, *Nucl. Phys. A* **261**, 174 (1976)
[65] Louis C Vaz *et al*, *Z. Phys. A* **315**, 169 (1984)
[66] E V Prokhorova *et al*, *Nucl. Phys. A* **802**, 45 (2008)
[67] C Ngo *et al*, *Z. Phys. A* **283**, 161 (1977)
[68] Z Zheng *et al*, *Nucl. Phys. A* **422**, 447 (1984)
[69] D J Morrissey *et al*, *Phys. Lett. B* **74**, 35 (1978)
[70] J Peter, C Ngo and B Tamain, *Nucl. Phys. A* **250**, 351 (1975)
[71] Katsuhisa Nishio, *J. Phys*. **312**, 82007 (2011)
[72] M Gitkis *et al*, *Nucl. Phys. A* **834** (2010)
[73] J Toke *et al*, *Nucl. Phys. A* **440**, 327 (1985)
[74] J Toke *et al*, *Phys. Lett. B* **142**, 258 (1984)
[75] K Nishio *et al*, *Eur. Phys. J. A* **29**, 281 (2006)
[76] G Franz *et al*, *Z. Phys. A* **291**, 167 (1979)